THE JOURNAL OF PHYSICAL CHEMISTRY B

Article

Cite This: J. Phys. Chem. B 2019, 123, 9355−9363

pubs.acs.org/JPCB

Hydrocarbon Chain-Length Dependence of Solvation Dynamics in Alcohol-Based Deep Eutectic Solvents: A Two-Dimensional Infrared Spectroscopic Investigation

Srijan Chatterjee,[§] Deborin Ghosh,[§] Tapas Haldar,[§,‡] Pranab Deb,[§,‡] Sushil S. Sakpal,[§,‡] Samadhan H. Deshmukh,[§,‡] Somnath M. Kashid,*[,§,‡] and Sayan Bagchi*[,§,‡]

[§]Physical and Materials Chemistry Division, CSIR-National Chemical Laboratory, Pune 411008, India

[‡]Academy of Scientific and Innovative Research (AcSIR), Ghaziabad 201002, India

Supporting Information

ABSTRACT: Deep eutectic solvents (DESs) have gained popularity in recent years as an environmentally benign, inexpensive alternative to organic solvents for diverse applications in chemistry and biology. Among them, alcohol-based DESs serve as useful media in various applications due to their significantly low viscosity as compared to other DESs. Despite their importance as media, little is known how their solvation dynamics change as a function of the hydrocarbon chain length of the alcohol constituent. In order to obtain insights into the chain-length dependence of the solvation dynamics, we have performed two-dimensional infrared spectroscopy on three alcohol-based DESs by systematically varying the hydrocarbon chain length. The results reveal that the solvent dynamics slows down monotonically with an increase in the chain length. This increase in the dynamic timescales also shows a strong correlation with the concomitant increase in the viscosity of DESs. In addition, we have performed molecular dynamics simulations to compare with the experimental results, thereby testing the capacity of simulations to determine the amplitudes and timescales of the structural fluctuations on fast timescales under thermal equilibrium conditions.

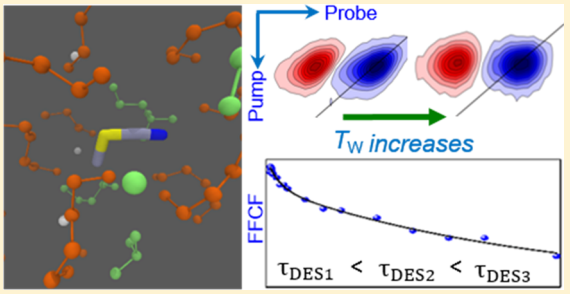

1. INTRODUCTION

Deep eutectic solvents (DESs), a neoteric class of designer solvents, have emerged as a popular alternative to conventional solvents in the last decade. Since the first report on DESs by Abbott et al.,[1] DESs have attracted considerable attention in diverse fields of chemistry, which include organic synthesis,[2,3] catalysis,[4] biotransformations,[5] extraction of metals,[6,7] carbon dioxide adsorption,[8] and electrochemistry.[9,10] A typical DES generally consists of a mixture of a hydrogen-bond (H-bond) donor and H-bond acceptor mixed in a certain mole ratio. Owing to interspecies H-bonds, a DES shows a large depression of its melting point as compared to that of its individual constituents and forms a stable solvent at room temperature.[11,12] DESs, though not strictly ionic in nature, are analogous to ionic liquids in terms of low vapor pressure, eco-friendliness, high conductivity, and low toxicity.[11,12] In addition, DESs have some intrinsic advantages as they are inexpensive and easy to synthesize. A large number of DESs with the desirable properties can be prepared by mixing the appropriately selected individual constituents as well as by varying their molar ratios.[13] The most commonly used DESs are composed of quaternary ammonium (like choline chloride (ChCl)) salts as the H-bond acceptors and amides, acids, and alcohols as H-bond donors.[13]

The solvation structure, interaction, and dynamics in various DESs have been investigated in recent years using both theory and experiments.[14−22] Information on solvation dynamics has been commonly obtained from molecular dynamics (MD) simulations and time-resolved fluorescence spectroscopy using molecular dyes.[17,23] Very recently, it has been shown that time-resolved infrared (IR) studies have some intrinsic advantages over molecular dyes,[24] and two-dimensional infrared (2D IR) spectroscopic studies of DESs have been reported.[24−26] The use of a vibrational probe, sensitive to the local environment, provides site-specific local information. Although DESs are analogous to ionic liquids in terms of low vapor pressure and conductivity, 2D IR reports on DESs are far less than those on ionic liquids.[27,28] Cui et al. investigated the dynamic processes in three different DESs consisting of urea, ethylene glycol, and glycerol as H-bond acceptors using a thiocyanate ion as the vibrational probe.[24] Another recent work used a nonionic DES composed of *N*-methylacetamide and lauric acid to understand the molecular heterogeneities produced by nanosegregation of the different domains of the eutectic mixture.[25]

Received: September 20, 2019
Revised: October 11, 2019
Published: October 14, 2019

DOI: 10.1021/acs.jpcb.9b08954
J. Phys. Chem. B 2019, 123, 9355−9363

A possible drawback when using DESs in applications is their high viscosity. Changes in macroscopic properties like hydrophobicity and viscosity are driven by molecular-level changes in structure and dynamics. Among all DESs, the significantly lower viscosity of alcohol-based DESs makes them quite useful as media in various applications.[11,12,29] It has been reported that an increase in the hydrocarbon chain length of the alcohols leads to a larger viscosity of the DES. However, little is known about the effect of chain length on the structure and dynamics of alcohol-based DESs. Samanta and co-workers have studied the effect of chain length and hydroxyl group positioning on the diffusion dynamics in alcohol-based DESs using time-resolved fluorescence spectroscopy.[30] As 2D IR spectroscopy is a powerful experimental technique to investigate the fast structural fluctuations of the solvent as sensed by a solute, a deeper understanding of the solvation dynamics of alcohol-based DESs can be obtained from 2D IR experiments.

In this work, we have used the nitrile (CN) stretch mode of methyl thiocyanate (MeSCN) as the IR probe to study the solvation dynamics in three DESs consisting of ChCl and alcohols of varying hydrocarbon chain lengths (Scheme 1).

Scheme 1. Compositions of Alcohol-Based DESs with Varying Hydrocarbon Chain Lengths

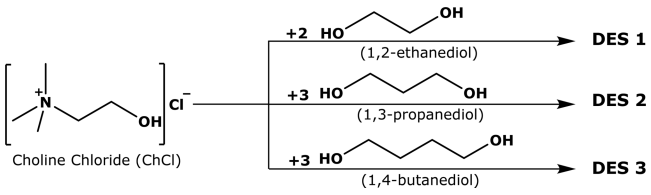

The CN stretch of thiocyanate has been used as it has been previously reported to have a long vibrational lifetime. Even though these alcohol-based DESs are less viscous than DESs consisting of other H-bond donors, these alcohol-based DESs have much higher viscosities than those of common organic solvents (viscosity of <1 cP). Therefore, a probe with a large vibrational lifetime is preferred to investigate the solvation dynamics of these DESs. The experimental measurements are made using IR absorption spectroscopy and 2D IR spectroscopy. The frequency−frequency correlation function (FFCF) in DES 1, DES 2, and DES 3, which connects the experimental observables to the underlying structural and fluctuation dynamics, is extracted from the waiting time dependence of the 2D IR spectra using the center line slope (CLS) method. Our results show that the solvation dynamics becomes slower with an increase in the hydrocarbon chain lengths of the alcohol constituent in the DES. As an increase in chain length leads to a concomitant increase in the DES viscosity, the solvation dynamics is found to have a strong correlation with viscosity. The fluctuation dynamics in all the DESs is also studied using MD simulations. Theoretical FFCFs are extracted, and the IR absorption spectra are constructed for all three DESs following a detailed analysis of the MD trajectories. The MD simulation results are compared with those from IR absorption and 2D IR spectroscopy experiments.

2. MATERIALS, METHODS, AND PROCEDURES

2.1. Materials. MeSCN, ChCl, 1,2-ethanediol, 1,3-propanediol, and 1,4-butanediol are purchased from Sigma-Aldrich. All these chemicals except ChCl are used without further purification.

2.2. Samples Preparation. All DESs are synthesized by following a reported procedure.[31] ChCl is dried in a vacuum oven at 90 °C for 24 h. All of the DESs are prepared by mixing ChCl to the respective alcohols at a specific molar ratio (Scheme 1) in an argon filled glovebox. The mixtures are heated and stirred at 60−70 °C until fully homogeneous colorless liquids are formed. Then, the reaction mixture is allowed to cool to room temperature for the experimental measurements.

2.3. Linear IR Spectroscopy. IR absorption spectra are measured on a Bruker Vertex 70 FTIR spectrometer with a 2 cm^{-1} resolution at room temperature. For each sample, ∼100 μL of the sample solution is loaded into a demountable cell (PIKE Technologies) consisting of two windows (CaF_2, 3 mm thickness, Shenzen Laser) separated by a mylar spacer of 100 μm thickness.

2.4. 2D IR Spectroscopy. In recent years, the nonlinear 2D IR spectroscopy has evolved as a powerful experimental technique to study ultrafast dynamics.[32,33] The 2D IR spectra reported in this work are collected by using a pulse shaper-based 2D IR spectrometer developed by Zanni and co-workers (Phasetech).[34] A Ti:sapphire regenerative amplifier (Libra, Coherent) outputs 800 nm, 50 fs pulses at a rate of 1 kHz, which pumps an optical parametric amplifier (OPA, OPerA Solo, Coherent). Signal (1367 nm) and idler (1929 nm) waves undergo difference frequency generation to produce mid-IR pulses. Mid-IR pulses of ∼80 fs duration with approximately 12 μJ of energy, 170 cm^{-1} in bandwidth, and centered at ∼2170 cm^{-1} are split into the pump (80%) and probe (20%) beams with a beam splitter. The pump pulse passes through a germanium acousto-optic modulator (AOM)-based pulse shaper.[34] The pulse shaper generates a collinear pair of compressed pump pulses with variable delays (τ) that are scanned to generate the pump axis of the 2D IR spectra. The pump and probe pulses are spatially overlapped (waiting time, T_w) and focused at the sample position using parabolic mirrors. At a fixed temporal delay between the pump and the probe pulses (waiting time, T_w), τ is scanned to generate the 2D IR signal. Four-frame phase cycling has been used to suppress pump scatter from the heterogeneous DES system. The signal was dispersed with a monochromator (Princeton Instruments) and detected on a liquid nitrogen-cooled 64 element mercury cadmium telluride (MCT) array IR detector (InfraRed Associates), which determines the probe axis (ω_t) of the 2D IR spectra. The 2D IR experimental data at a fixed T_w is a function of the variable delay time between the two pump pulses (τ) and probe frequencies (ω_t). Numerical Fourier transform at each ω_t gives the second frequency variable, ω_τ. The results are plotted as a two-dimensional spectrum (contour plot) with frequency variables ω_τ and ω_t. A 2D spectrum is obtained for each waiting time, T_w. All 2D IR spectra are recorded at 22 °C temperature. The sample cells for 2D IR experiments are prepared in the same manner as that for IR absorption experiments.

2.5. Molecular Dynamics Simulation. Classical molecular dynamics simulation is conducted on GROMACS 2016.5 package.[35] Parameters for MeSCN are derived from quantum chemical calculation followed by RESP charge fitting by ANTECHAMBER software to produce the general AMBER force field.[36] This force field has been widely tested[37] and has been previously used by Cho and co-workers for parameter-

DOI: 10.1021/acs.jpcb.9b08954
J. Phys. Chem. B 2019, 123, 9355−9363

ization of MeSCN.[38] Several other pioneering works by Corcelli et al. and Thompson et al. also report on CN parameterization albeit not of a molecule containing a thiocyanate group.[39,40] Parameters for DESs 1, 2, and 3 are taken from the work of Doherty et al.[41] and the automatic server by Jorgensen and co-workers.[42] Simulation boxes are defined by one molecule of MeSCN, 200 choline chloride ion pairs, and a varying number of alcohols by maintaining the experimental DES composition ratio. Energy minimization by the steepest descent algorithm with a 2 fs step size is performed prior to each simulation step. For short-range electrostatic interactions, a periodic boundary condition with a cutoff of 16 Å is used. An *NVT* ensemble in 300 K for 1 ns with a velocity rescale thermostat and subsequently *NPT* ensemble at 300 K and 1 bar using a Parrinello−Rahman barostat for 5 ns are performed. LINCS is used to constrain all covalently bonded hydrogen atoms. Production runs are carried out for 50 ns. The electric field on nitrile of methyl thiocyanate is calculated according to our previous work.[43] A hydrogen bond analysis is performed on GROMACS with the last 5 ns of each trajectory where a distance cutoff of 3.5 Å and an angle cutoff of 30° are used. Similar cutoff values for DES have been reported earlier.[44,45] In order to determine the autocorrelation function, five independent additional production runs of 500 ps with a 4 fs interval for data output and subsequent electric field calculation are performed. The electric field autocorrelation function is determined using the GROMACS built-in tool from electric field data and averaged over five independent runs. Furthermore, to compare the MD results with another force field, we have also used a general AMBER force field to calculate parameters of ChCl of the DESs.[36]

3. RESULTS AND DISCUSSION

3.1. Linear IR Spectroscopy. The IR absorption spectra of the CN stretching mode of MeSCN in DES 1, DES 2, and DES 3 show single symmetric bands. Apparently, the peak shapes and the peak maxima (~2155 cm^{-1}) are almost identical in all three DESs (Figure 1). The CN stretch band in

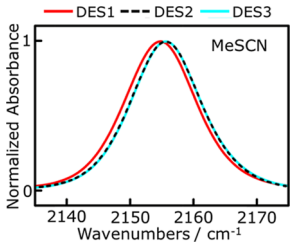

Figure 1. Normalized IR absorption spectra of the CN stretch mode of MeSCN in DES 1 (red), DES 2 (dashed black), and DES 3 (cyan). The actual absorbance for each sample is ~0.1.

any DES can be fitted well with a Gaussian line shape function. Gaussian fits indicate a small blueshift with increasing hydrocarbon chain lengths of the alcohol constituent of the DESs. The peak positions and the full width at half maximum (FWHM) of the fitted peaks are given in Table 1. Although there is a gradual increase in the viscosity of the DESs with increasing alcohol chain length, only small differences can be observed in the steady-state IR spectrum.

It has been well established that nitriles, when exposed to water can accept an H-bond causing a blueshift of the nitrile

Table 1. Peak Positions and Full Width at Half Maximum (FWHM) of the Fitted FTIR Signals of MeSCN in All Three DESs[a]

DES	IR peak frequency (cm^{-1})	FWHM (cm^{-1})	viscosity (cP)[b]
DES 1	2154.8	14.06	30.0
DES 2	2155.6	13.84	53.0
DES 3	2155.7	13.80	84.5

[a]The reported viscosities of these DESs are also presented. [b]The values are taken from ref 30.

stretching frequency.[46−50] When dissolved in an alcohol (methanol), nitrile exists in both H-bonded and non-H-bonded forms, which interconvert in a picosecond timescale.[51] Even though the hydroxyl (OH) group is present in both the ChCl and alcohol in DESs 1−3, the H-bonding status of the CN probe in these DESs is not known a priori. A recent study on the thiocyanate ion reported theoretical evidence of H-bonding in DES 1 occurring primarily from the sulfur end where the negative charge of the anion is localized.[24] However, a neutral thiocyanate group, attached covalently to the methyl carbon of MeSCN, has been used as the IR probe in the present study. Thus, MD simulations are needed to obtain further information about the H-bonding status of the IR probe.

3.2. 2D IR Spectroscopy. Two-dimensional IR spectra of the CN stretching mode of MeSCN in DES 1, DES 2, and DES 3 are measured at different waiting times (T_w). Figure 2 shows representative 2D IR spectra in the three DESs at four T_w delays. The 2D IR spectra consist of a pair of peaks arising from the 0−1 transition (ground-state bleach and excited-state stimulated emission, blue) on the diagonal axis (ω_τ = 2155 cm^{-1} and ω_t = 2155 cm^{-1}) and 1−2 transition (excited-state absorption, red) shifted along the horizontal axis (ω_τ = 2155 cm^{-1} and ω_t = 2127 cm^{-1}) by the vibrational anharmonicity of the CN stretching mode. The vibrational anharmonicity is estimated to be almost constant (~28 cm^{-1}) in all three DESs. Our results agree well with the earlier reported anharmonicity of the CN probe in MeSCN.[52−55] With the increase in T_w, vibrational lifetime (T_1) causes the 2D IR peaks to decay. T_1 can be independently estimated using IR pump−probe experiments. The estimated values of T_1 in DESs 1, 2, and 3 are ~68 ps, almost constant within the experimental error bar.

The 2D IR peak positions remain fixed with the increase in T_w; however, the shapes of the peaks change. The evolution of the peak shape with increasing waiting time is the manifestation of the effect of solvent dynamics, also known as spectral diffusion. In all three DESs, the peaks are elongated along the diagonal at shorter T_w values and become more symmetrical and less elongated as T_w increases. It is apparent from Figure 2 that the 2D IR peak shape at a large T_w becomes less symmetrical as we go on from smaller-chain alcohols to larger-chain ones. This trend apparently indicates that the solvent-induced fluctuation occurs at a slower timescale with an increase of hydrocarbon chain length in the alcohol constituent of the DES. However, a detailed analysis of the T_w dependence of the 2D line shapes is needed to determine the timescales and amplitudes of frequency fluctuations in the CN mode that are associated to the solvation dynamics of the DESs.

3.3. FFCF Analysis. The FFCF quantifies the connection between the waiting time evolution of the 2D IR peak shapes and the amplitudes and timescales of the frequency

DOI: 10.1021/acs.jpcb.9b08954
J. Phys. Chem. B 2019, 123, 9355−9363

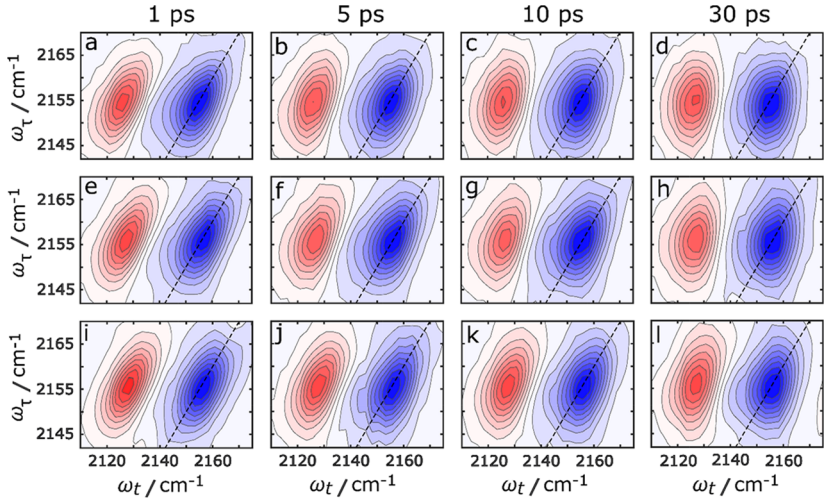

Figure 2. 2D IR spectra of (a–d) DES 1, (e–h) DES 2, and (i–l) DES 3 at T_w = 1, 5, 10, and 30 ps.

fluctuations caused by the DES dynamics. Different analysis strategies (nodal line slope, ellipticity, diagonal and anti-diagonal widths, and central line slope (CLS)) have been previously utilized to extract the FFCF information from the 2D IR spectra. In this work, we have used the CLS formalism to determine the FFCF from the 2D IR and IR absorption spectra in all three DESs. The CLS is a normalized function closely related to the FFCF with decay times the same as those in the FFCF. Figure 3 shows the T_w-dependent CLS data for the CN stretch mode of MeSCN in DES 1, DES 2, and DES 3. In the absence of any homogeneous broadening at T_w = 0, the value of the CLS should be 1. The CLS curves for the CN probe dissolved in DESs 1–3 (Figure 3) begin at a value of ~0.65. This difference between 1 and the initial value of CLS is

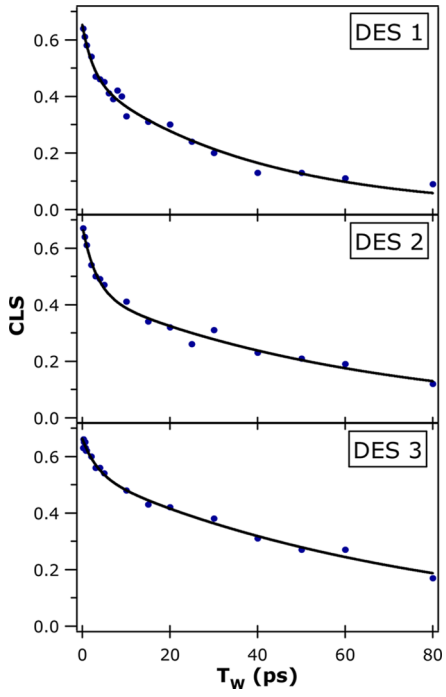

Figure 3. T_w-dependent CLS for CN stretch of MeSCN in three different deep eutectic solvents. The blue dots are the data, and the black curves are biexponential fits. The difference from 1 at T_w = 0 is related to the homogeneous line width.

related to the magnitude of the homogeneous contribution to the line shapes of the IR absorption and 2D IR spectra, arising from the motionally narrowed component produced by very fast fluctuations. Other homogeneous contributions arise from T_1 (measured independently) and orientational relaxation (T_{or}). The effect of T_{or} is neglected in this study due to the high viscosity of the DESs.[12,24] However, reorientation-induced spectral diffusion (RISD) has been previously reported in viscous liquids.[56] Polarization dependent T_w data (Figure S1 and Table S1) confirm the absence of RISD. The CLS gives the normalized FFCF, but the CLS method[57,58] additionally allows extraction of the complete FFCF, which includes the frequency fluctuation amplitudes and the homogeneous line width. The FFCF is modeled with the form

$$C(t) = \langle \delta\omega(t)\delta\omega(0)\rangle = \frac{\delta(t)}{T_2} + \sum_{i=1}^{n} \Delta_i^{\,2} e^{-t/\tau_i} + \Delta_S^{\,2} \quad (1)$$

In eq 1, Δ_i and τ_i are the CN frequency fluctuation amplitude and timescale, respectively, induced by DES structural dynamics for the ith component. For a motionally narrowed term with $\Delta\tau < 1$, Δ and τ cannot be determined separately. The motionally narrowed contribution to the absorption spectrum has a pure dephasing line width given by $\Gamma^* = \Delta^2\tau = 1/\pi T_2^*$ where T_2^* is the pure dephasing time. The total homogeneous line width is estimated by $\Gamma = 1/\pi T_2$ where T_2 is the total homogeneous dephasing time given by $1/T_2 = 1/T_2^* + 1/2T_1$.

After a certain waiting time when the probe has sampled all the possible configurations, the CLS should decay to 0. Figure 3 shows that CLS in all three DESs decay to ~0.1 at 80 ps. The CLS data in all DESs are fit with a biexponential function with and without an offset (Δ_S). In the fits that include an adjustable offset, the fits converge with an offset of ~0. Thus, the fits shown in Figure 3 do not include an offset. An offset would indicate that solvent fluctuations are too slow to contribute to the experimental time window of 80 ps. Our results suggest that DES fluctuations much slower than ~200 ps comprise at most a small percent of the CN absorption spectrum.

The homogeneous contribution and the total inhomogeneous line width (from the absolute value of the Δ_i's) are determined through a simultaneous fit to the IR absorption line shape and the T_w dependence of the CLS, resulting in the

DOI: 10.1021/acs.jpcb.9b08954
J. Phys. Chem. B 2019, 123, 9355–9363

Table 2. CLS Parameters from 2D IR Experiments

DES	T_2* (ps)	Γ (cm^{-1})	Δ_1 (cm^{-1})	τ_1 (ps)	Δ_2 (cm^{-1})	τ_2 (ps)	Δ_{inhomo} (cm^{-1})
DES 1	2.7	3.8	2.4 ± 0.2	2.5 ± 0.8	4.1 ± 0.1	38.4 ± 3.3	4.8
DES 2	3.1	3.3	2.7 ± 0.1	3.2 ± 0.7	3.8 ± 0.1	65.3 ± 6.8	4.7
DES 3	3.2	3.2	1.9 ± 0.2	3.5 ± 0.9	4.3 ± 0.1	75.5 ± 4.5	4.7

full FFCF (eq 1). The decay time constants, the frequency fluctuation amplitudes, homogeneous and inhomogeneous line widths, and pure dephasing times (T_2*) are given in Table 2. Γ is the FWHM of the Lorentzian homogeneous line, and the fluctuation amplitudes (Δ_1 and Δ_2) are standard deviations of the Gaussian line shape associated with each contribution to the inhomogeneous broadening. The total inhomogeneous line width is given by the convolution of the two Gaussian line shapes, $\Delta_{inhomo} = \sqrt{\Delta_1^2 + \Delta_2^2}$. The FWHM of the total inhomogeneous line is given by $2.35\Delta_{inhomo}$. It is observed that inhomogeneous broadening is predominant (~65−70%) in the absorption spectra of all three DESs and contributes to ~11 cm^{-1} to the FWHM in the absorption spectra for all three DESs. The almost uniform homogeneous contribution (~30−35%) also corroborates with the almost uniform initial drop to ~0.65 in the normalized CLS data for all three DESs at $T_w = 0$. Moreover, the FFCF analysis also shows that the overall broadening from the Lorentzian and the Gaussian components almost remains constant as a function of alcohol chain length. This explains the almost identical IR absorption spectra shown in Figure 1. However, a major difference can be observed in the fluctuation timescales.

In all three DESs, a fast timescale of ~3.5 ps is observed within the experimental errors. The other timescale (τ_2), obtained from the CLS fit, is much slower and increases from DES 1 to DES 3. An earlier report on a thiocyanate anion dissolved in DESs also observed a fast and a slow component[24] in the timescales. A plausible reason for the slowing down of the solvent dynamics with an increase in the hydrocarbon chain lengths is the DES viscosity (Table 1).[24] The slower timescale in DES has been previously assigned to the diffusion of the DES constituents exchanging in and out of the solvation shell of the solute. The timescales of the diffusional motions depend on DES viscosity. Figure S2 shows a monotonic increase of τ_2 with the increase in the DES viscosities. The fast component in the solvation dynamics can be assigned to solvent fluctuations within the first solvation shell without any significant change in the center of mass of the molecule. It has been previously shown for non-H-bonded nitriles attached to biomolecules[49,59−67] that a fluctuating electrostatic model in conjunction to a vibrational Stark effect is useful to compute the IR absorption spectra and compare the fluctuation timescales obtained from CLS fits.

3.4. Molecular Dynamics Simulation. H-bonding analysis is performed on the simulation trajectories. The nitrogen (N) of the MeSCN is found to be predominantly non-H-bonded. Only ~5% of the MD snapshots are H-bonded in DES 1, and the H-bonding propensity decreases with the increase in the alcohol chain length. Varying the H-bond cutoff parameters does not make large changes in the H-bonded population. The increased hydrophobicity arising from the larger hydrocarbon chain length might provide a plausible explanation for this trend. For further validation, we have estimated the average electrostatic fields from the MD trajectories exerted by DESs 1−3 along the CN bond, which were evaluated at the midpoint of the bond. The magnitudes of the average electric field show a slight decrease with the increase in alcohol chain length (Table S2). It has been reported previously for MeSCN that a decrease in the electric field is accompanied by an increase in the nitrile IR frequencies for non-H-bonded nitriles.[46] We also observe a similar relation between CN IR frequencies and the estimated electric fields. This further validates the non-H-bonding status of the CN probe in the alcohol-based DESs and allows us to employ the electrostatic model to link the spectroscopic observable to MD trajectories.[59,68]

In this model, the local electric field at the ligand induces an instantaneous frequency shift in the CN vibrational frequency (vibrational Stark effect). As the structure fluctuates, the electric field along the CN bond fluctuates. This frequency fluctuation is given by

$$\delta\omega(t) = \lambda[\vec{u}(t)\cdot\vec{E}(t) - \langle\vec{u}\cdot\vec{E}\rangle] \quad (2)$$

In eq 2, $\vec{u}(t)$ is a unit vector pointing along the CN bond, and the angle brackets denote an equilibrium average. The parameter λ plays the role of a microscopic version of the Stark tuning rate. Thus, the autocorrelation of the electric field multiplied by λ provides the FFCF. The MD simulations are independent of λ; however, λ allows us to convert the simulated electric fields to spectroscopic frequencies. As the fluctuation in frequency is linear in λ, the FFCF ($C(t) = \langle\delta\omega(t)\delta\omega(0)\rangle$) is quadratic in λ. Varying λ corresponds only to changing the amplitude factors of $C(t)$ (see eq 1), leaving the decay times unchanged.

IR absorption line shapes for all three DESs, shown in Figure 4, are calculated from simulated FFCFs. The simulations yield line shapes but do not provide absolute frequencies. The center frequencies of the simulated spectra are aligned with the corresponding experimental peak frequencies to facilitate the comparison of the line shapes. The coupling parameter λ is the single adjustable parameter relating simulation results to the experimental data to give the best fit to the line shapes. The values of λ obtained are 0.49, 0.55, and 0.5 cm^{-1}/(MV/cm) for DESs 1−3, respectively. These values are almost 65−75% of the experimentally measured Stark tuning rate, 0.72 cm^{-1}/(MV/cm), for a thiocyanate probe.[69] However, it has been recently reported that the experimental Stark tuning rate contains a local field factor arising from the frozen matrix and therefore overestimates the λ by a factor of 1.0 to 2.[70−74] Thus, the values of λ obtained from the spectral fit agree well with the reported Stark tuning rate obtained from independent vibrational Stark experiments. The fact that λ values obtained from simulation and fit to the IR absorption line shapes are in good agreement with the experimentally measured Stark tuning rate strongly supports the fluctuating electric field (Stark) model that relates the global solvation dynamics of the DES systems as sensed by the CN probe to 2D IR variables.

The theoretically estimated FFCFs (Figure 5) can be fitted to the triexponential form

DOI: 10.1021/acs.jpcb.9b08954
J. Phys. Chem. B 2019, 123, 9355−9363

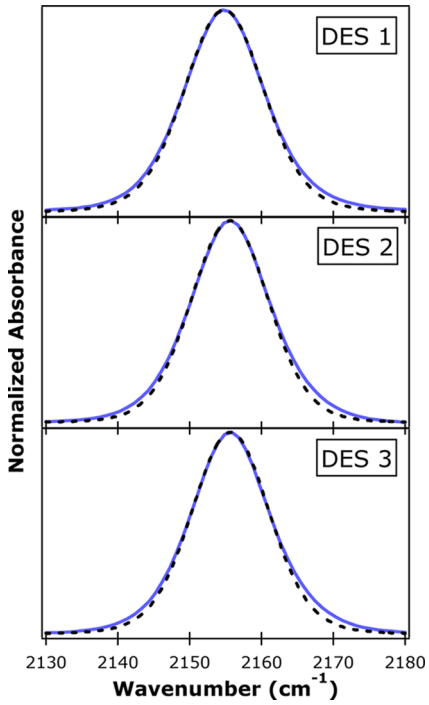

Figure 4. Normalized IR absorption spectra of MeSCN in three different DESs calculated from simulated FFCFs (dashed black curves) are compared to the experimental spectra (blue curves). To compare line shapes, the peak frequencies of the simulated peaks are aligned with those of the experimental spectra. A single adjustable parameter, λ, is used to simultaneously fit both bands (see text).

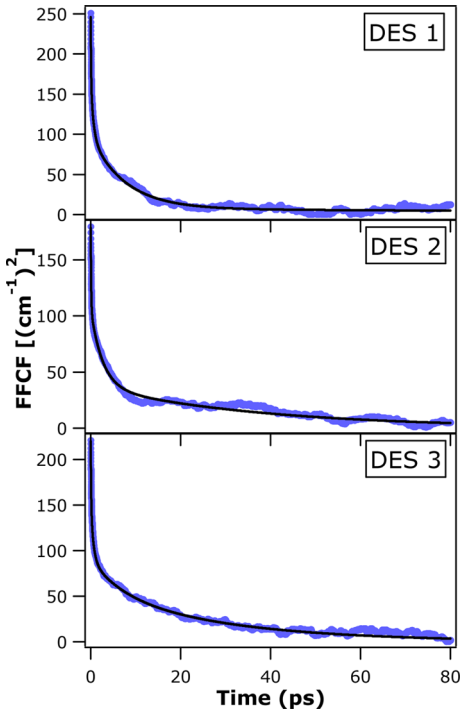

Figure 5. FFCFs (blue) of MeSCN in DES 1, DES 2, and DES 3 obtained from MD simulations. The black curves are the triexponential fits to the FFCSs

$$C(t) = \Delta_f^{\,2} e^{-t/\tau_f} + \sum_{i=1}^{n} \Delta_i^{\,2} e^{-t/\tau_i} + \Delta_S^{\,2}$$

to extract the solvation dynamics timescales in all three DESs. As the FFCF decays to ~0 within 80 ps, the offset (Δ_S) was not used in the fitting. The first rapid decays (τ_f) are complete in a few hundred femtoseconds. These initial decays cannot be measured from 2D IR spectra as they give rise to the homogeneous component (T_2). These rapid decays are followed by slower time evolutions, τ_1 and τ_2. All the timescales obtained from the fits are given in Table S3. It can be seen that the relative trends in MD-estimated τ_1 and τ_2 agree with those measured from 2D IR experiments as a function of alcohol chain length. This is also apparent from Figure S2 where the monotonic increase in τ_2 with DES viscosity is observed from both experiments and theory. However, the absolute values of the timescales (τ_1 and τ_2) obtained from MD simulations do not show a good match with those obtained from experiments. Similar mismatches between the experimental and theoretical fluctuation timescales have been previously reported for nitrile probes attached to a protein.[59] Interestingly, similar to our findings in this report, the calculated IR absorption spectra from the MD-estimated FFCF in those reports showed excellent agreement with the experimental spectra. As the simulated IR absorption spectra depend on the relative amplitudes of the different components and λ, the FWHM of the simulated spectra agrees well with the experimental spectra. It is possible that the potential energy landscape determined by an MD force field is more (less) rugged with higher (lower) energy barriers than that existing in real systems. Furthermore, we have compared the results from MD simulations using another force field. The values of λ obtained using the different force field are 0.65, 0.52, and 0.5 $cm^{-1}/(MV/cm)$ for DESs 1−3, respectively. These values, though they show a qualitative agreement with the Stark tuning rate, have a larger spread than the values of λ reported earlier. The timescales (Table S4) obtained from the triexponential fitting of the theoretically estimated FFCF(s) show the same general trend as obtained in the 2D IR experiment. However, these timescales are much slower as compared to those estimated using the other force field. As MD simulations are being routinely used to predict solvation microheterogeneity of various DESs, our results show that the MD force fields of heterogeneous DESs need to be properly benchmarked. The picosecond solvation dynamics timescales obtained from 2D IR experiments would allow a direct comparison of the simulation and experimental results, thereby providing a platform to benchmark the force fields.

Radial distribution functions (RDF, Figure S3) show a strong interaction between MeSCN and the quaternary nitrogen atom of the choline cation. Based on a previous report of MeSCN interacting with another cation,[55] we surmise that this electrostatic interaction inhibits small angular wobbling of the vibrational probe occurring on a timescale that is fast compared to the motion of the surrounding ion. This might be the plausible reason why polarization-dependent T_w data show almost identical CLS values in 2D IR experiments performed with parallel and perpendicular polarizations.

4. CONCLUSIONS

In this work, we report a 2D IR study of the solvation dynamics of three alcohol-based DESs with varying hydrocarbon chain lengths. Although the steady-state IR absorption spectra of MeSCN apparently cannot distinguish between the DESs, the time-resolved 2D IR spectroscopy clearly can differentiate the DESs based on solvation dynamics timescales.

DOI: 10.1021/acs.jpcb.9b08954
J. Phys. Chem. B 2019, 123, 9355−9363

The solvation dynamics of all three DES has an ultrafast decay component that gives rise to a motionally narrowed component followed by a fast decay component and a slower component. The slowest fluctuation timescale monotonically increases with increasing hydrocarbon chain length in the alcohol-based DES and shows a strong correlation with the DES viscosity. We have also performed MD simulations and compared the simulation results to those from experiments. The simulations produce dynamics that shows the same relative trends as a function of alcohol chain length, however, do not show a great match with the absolute values of the experimentally obtained timescales. However, the simulations do a good job of reproducing the IR absorption spectra in all three DESs.

■ ASSOCIATED CONTENT

Supporting Information

The Supporting Information is available free of charge on the ACS Publications website at DOI: 10.1021/acs.jpcb.9b08954.

Simulation methodology and analysis details (PDF)

■ AUTHOR INFORMATION

Corresponding Authors

*E-mail: kashidsm@gmail.com (S.M.K.).
*E-mail: s.bagchi@ncl.res.in (S.B.).

ORCID

Sayan Bagchi: 0000-0001-6932-3113

Notes

The authors declare no competing financial interest.

■ ACKNOWLEDGMENTS

Authors acknowledge SERB India (nos. EMR/2016/001069 and EMR/2016/000576), and P.D. thanks DST-Inspire for the fellowship. We would like to thank Debranjan Mandal and Abhijit Bera CSIR-NCL, Pune for their support in DES synthesis.

■ REFERENCES

(1) Abbott, A. P.; Capper, G.; Davies, D. L.; Rasheed, R. K.; Tambyrajah, V. Novel solvent properties of choline chloride/urea mixtures. *Chem. Commun.* **2003**, 70−71.

(2) Alonso, D. A.; Baeza, A.; Chinchilla, R.; Guillena, G.; Pastor, I. M.; Ramón, D. J. Deep eutectic solvents: The organic reaction medium of the century. *Eur. J. Org. Chem.* **2016**, *2016*, 612−632.

(3) Ruß, C.; König, B. Low melting mixtures in organic synthesis − an alternative to ionic liquids? *Green Chem.* **2012**, *14*, 2969−2982.

(4) Gu, Y.; Jérôme, F. Bio-based solvents: an emerging generation of fluids for the design of eco-efficient processes in catalysis and organic chemistry. *Chem. Soc. Rev* **2013**, *42*, 9550−9570.

(5) Gorke, J. T.; Srienc, F.; Kazlauskas, R. J. Hydrolase-catalyzed biotransformations in deep eutectic solvents. *Chem. Commun.* **2008**, 1235−1237.

(6) Abbott, A. P.; Capper, G.; Davies, D. L.; Rasheed, R. K.; Shikotra, P. Selective extraction of metals from mixed oxide matrixes using choline-based ionic liquids. *Inorg. Chem.* **2005**, *44*, 6497−6499.

(7) Abbott, A. P.; Boothby, D.; Capper, G.; Davies, D. L.; Rasheed, R. K. Deep eutectic solvents formed between choline chloride and carboxylic acids: versatile alternatives to ionic liquids. *J. Am. Chem. Soc.* **2004**, *126*, 9142−9147.

(8) Leron, R. B.; Li, M.-H. Solubility of carbon dioxide in a choline chloride−ethylene glycol based deep eutectic solvent. *Thermochim. Acta* **2013**, *551*, 14−19.

(9) Nkuku, C. A.; LeSuer, R. J. Electrochemistry in deep eutectic solvents. *J. Phys. Chem. B* **2007**, *111*, 13271−13277.

(10) Jhong, H.-R.; Wong, D. S.-H.; Wan, C.-C.; Wang, Y.-Y.; Wei, T.-C. A novel deep eutectic solvent-based ionic liquid used as electrolyte for dye-sensitized solar cells. *Electrochem. Commun.* **2009**, *11*, 209−211.

(11) Zhang, Q.; De Oliveira Vigier, K.; Royer, S.; Jérôme, F. Deep eutectic solvents: syntheses, properties and applications. *Chem. Soc. Rev.* **2012**, *41*, 7108−7146.

(12) Smith, E. L.; Abbott, A. P.; Ryder, K. S. Deep eutectic solvents (DESs) and their applications. *Chem. Rev.* **2014**, *114*, 11060−11082.

(13) Francisco, M.; van den Bruinhorst, A.; Kroon, M. C. Low-transition-temperature mixtures (LTTMs): A new generation of designer solvents. *Angew. Chem., Int. Ed.* **2013**, *52*, 3074−3085.

(14) Abbott, A. P.; Harris, R. C.; Ryder, K. S.; D'Agostino, C.; Gladden, L. F.; Mantle, M. D. Glycerol eutectics as sustainable solvent systems. *Green Chem.* **2011**, *13*, 82−90.

(15) D'Agostino, C.; Harris, R. C.; Abbott, A. P.; Gladden, L. F.; Mantle, M. D. Molecular motion and ion diffusion in choline chloride based deep eutectic solvents studied by 1H pulsed field gradient NMR spectroscopy. *Phys. Chem. Chem. Phys.* **2011**, *13*, 21383−21391.

(16) D'Agostino, C.; Gladden, L. F.; Mantle, M. D.; Abbott, A. P.; Ahmed, E. I.; Al-Murshedi, A. Y. M.; Harris, R. C. Molecular and ionic diffusion in aqueous − deep eutectic solvent mixtures: probing inter-molecular interactions using PFG NMR. *Phys. Chem. Chem. Phys.* **2015**, *17*, 15297−15304.

(17) Das, A.; Biswas, R. Dynamic solvent control of a reaction in ionic deep eutectic solvents: time-resolved fluorescence measurements of reactive and nonreactive dynamics in (choline chloride + urea) melts. *J. Phys. Chem. B* **2015**, *119*, 10102−10113.

(18) Matsugami, M.; Yoshida, N.; Hirata, F. Theoretical characterization of the "ridge" in the supercritical region in the fluid phase diagram of water. *J. Chem. Phys.* **2014**, *140*, 104511.

(19) Mukherjee, K.; Das, A.; Choudhury, S.; Barman, A.; Biswas, R. Dielectric relaxations of (acetamide + electrolyte) deep eutectic solvents in the frequency window, $0.2 \leq \nu/\mathrm{GHz} \leq 50$: anion and cation dependence. *J. Phys. Chem. B* **2015**, *119*, 8063−8071.

(20) Kaur, S.; Gupta, A.; Kashyap, H. K. Nanoscale spatial heterogeneity in deep eutectic solvents. *J. Phys. Chem. B* **2016**, *120*, 6712−6720.

(21) Fetisov, E. O.; Harwood, D. B.; Kuo, I. F. W.; Warrag, S. E. E.; Kroon, M. C.; Peters, C. J.; Siepmann, J. I. First-principles molecular dynamics study of a deep eutectic solvent: choline chloride/urea and its mixture with water. *J. Phys. Chem. B* **2018**, *122*, 1245−1254.

(22) Faraone, A.; Wagle, D. V.; Baker, G. A.; Novak, E. C.; Ohl, M.; Reuter, D.; Lunkenheimer, P.; Loidl, A.; Mamontov, E. Glycerol hydrogen-bonding network dominates structure and collective dynamics in a deep eutectic solvent. *J. Phys. Chem. B* **2018**, *122*, 1261−1267.

(23) Das, A.; Das, S.; Biswas, R. Density relaxation and particle motion characteristics in a non-ionic deep eutectic solvent (acetamide + urea): Time-resolved fluorescence measurements and all-atom molecular dynamics simulations. *J. Chem. Phys.* **2015**, *142*, No. 034505.

(24) Cui, Y.; Fulfer, K. D.; Ma, J.; Weldeghiorghis, T. K.; Kuroda, D. G. Solvation dynamics of an ionic probe in choline chloride-based deep eutectic solvents. *Phys. Chem. Chem. Phys.* **2016**, *18*, 31471−31479.

(25) Cui, Y.; Rushing, J. C.; Seifert, S.; Bedford, N. M.; Kuroda, D. G. Molecularly heterogeneous structure of a nonionic deep eutectic solvent composed of n-methylacetamide and lauric acid. *J. Phys. Chem. B* **2019**, *123*, 3984−3993.

(26) Cui, Y.; Kuroda, D. G. Evidence of molecular heterogeneities in amide-based deep eutectic solvents. *J. Phys. Chem. A* **2018**, *122*, 1185−1193.

(27) Nicolau, B. G.; Sturlaugson, A.; Fruchey, K.; Ribeiro, M. C. C.; Fayer, M. D. Room temperature ionic liquid−lithium salt mixtures: optical kerr effect dynamical measurements. *J. Phys. Chem. B* **2010**, *114*, 8350−8356.

(28) Canongia Lopes, J. N. A.; Pádua, A. A. H. Nanostructural organization in ionic liquids. *J. Phys. Chem. B* **2006**, *110*, 3330−3335.

DOI: 10.1021/acs.jpcb.9b08954
J. Phys. Chem. B 2019, 123, 9355−9363

(29) Cruz, H.; Jordão, N.; Branco, L. C. Deep eutectic solvents (DESs) as low-cost and green electrolytes for electrochromic devices. *Green Chem.* **2017**, *19*, 1653−1658.
(30) Hossain, S. S.; Samanta, A. How do the hydrocarbon chain length and hydroxyl group position influence the solute dynamics in alcohol-based deep eutectic solvents? *Phys. Chem. Chem. Phys.* **2018**, *20*, 24613−24622.
(31) Harris, R. C. *Physical properties of alcohol based deep eutectic solvents*; University of Leicester, 2008.
(32) Kim, Y. S.; Hochstrasser, R. M. Applications of 2D IR spectroscopy to peptides, proteins, and hydrogen-bond dynamics. *J. Phys. Chem. B* **2009**, *113*, 8231−8251.
(33) Ishikawa, H.; Kwak, K.; Chung, J. K.; Kim, S.; Fayer, M. D. Direct observation of fast protein conformational switching. *Proc. Natl. Acad. Sci. U. S. A.* **2008**, *105*, 8619−8624.
(34) Ghosh, A.; Serrano, A. L.; Oudenhoven, T. A.; Ostrander, J. S.; Eklund, E. C.; Blair, A. F.; Zanni, M. T. Experimental implementations of 2D IR spectroscopy through a horizontal pulse shaper design and a focal plane array detector. *Opt. Lett.* **2016**, *41*, 524−527.
(35) Abraham, M. J.; Murtola, T.; Schulz, R.; Páll, S.; Smith, J. C.; Hess, B.; Lindahl, E. GROMACS: High performance molecular simulations through multi-level parallelism from laptops to supercomputers. *SoftwareX* **2015**, *1-2*, 19−25.
(36) Wang, J.; Wolf, R. M.; Caldwell, J. W.; Kollman, P. A.; Case, D. A. Development and testing of a general amber force field. *J. Comput. Chem.* **2004**, *25*, 1157−1174.
(37) Caleman, C.; van Maaren, P. J.; Hong, M.; Hub, J. S.; Costa, L. T.; van der Spoel, D. Force field benchmark of organic liquids: density, enthalpy of vaporization, heat capacities, surface tension, isothermal compressibility, volumetric expansion coefficient, and dielectric constant. *J. Chem. Theory Comput.* **2012**, *8*, 61−74.
(38) Oh, K.-I.; Choi, J.-H.; Lee, J.-H.; Han, J.-B.; Lee, H.; Cho, M. Nitrile and thiocyanate IR probes: Molecular dynamics simulation studies. *J. Chem. Phys.* **2008**, *128*, 154504.
(39) Yamada, S. A.; Thompson, W. H.; Fayer, M. D. Water-anion hydrogen bonding dynamics: Ultrafast IR experiments and simulations. *J. Chem. Phys.* **2017**, *146*, 234501.
(40) Lindquist, B. A.; Corcelli, S. A. Nitrile Groups as Vibrational Probes: Calculations of the C≡N infrared absorption line shape of acetonitrile in water and tetrahydrofuran. *J. Phys. Chem. B* **2008**, *112*, 6301−6303.
(41) Doherty, B.; Acevedo, O. OPLS force field for choline chloride-based deep eutectic solvents. *J. Phys. Chem. B* **2018**, *122*, 9982−9993.
(42) Dodda, L. S.; Vilseck, J. Z.; Tirado-Rives, J.; Jorgensen, W. L. 1.14*CM1A-LBCC: Localized bond-charge corrected cm1a charges for condensed-phase simulations. *J Phys Chem B* **2017**, *121*, 3864−3870.
(43) Haldar, T.; Bagchi, S. Electrostatic Interactions Are Key to C═O n-π^* Shifts: An Experimental Proof. *J. Phys. Chem. Lett.* **2016**, *7*, 2270−2275.
(44) Shah, D.; Mjalli, F. S. Effect of water on the thermo-physical properties of Reline: An experimental and molecular simulation based approach. *Phys. Chem. Chem. Phys.* **2014**, *16*, 23900−23907.
(45) Shah, D.; Mansurov, U.; Mjalli, F. S. Intermolecular interactions and solvation effects of dimethylsulfoxide on type III deep eutectic solvents. *Phys. Chem. Chem. Phys.* **2019**, *21*, 17200−17208.
(46) Deb, P.; Haldar, T.; Kashid, S. M.; Banerjee, S.; Chakrabarty, S.; Bagchi, S. Correlating nitrile IR frequencies to Local electrostatics quantifies noncovalent interactions of peptides and proteins. *J. Phys. Chem. B* **2016**, *120*, 4034−4046.
(47) Reimers, J. R.; Hall, L. E. The solvation of acetonitrile. *J. Am. Chem. Soc.* **1999**, *121*, 3730−3744.
(48) Fafarman, A. T.; Sigala, P. A.; Schwans, J. P.; Fenn, T. D.; Herschlag, D.; Boxer, S. G. Quantitative, directional measurement of Electric Field heterogeneity in the active site of Ketosteroid Isomerase. *Proc. Natl. Acad. Sci. U. S. A.* **2012**, *109*, E299−E308.
(49) Getahun, Z.; Huang, C.-Y.; Wang, T.; De León, B.; DeGrado, W. F.; Gai, F. Using nitrile-derivatized amino acids as infrared probes of local environment. *J. Am. Chem. Soc.* **2003**, *125*, 405−411.
(50) Aschaffenburg, D. J.; Moog, R. S. Probing hydrogen bonding environments: solvatochromic effects on the CN vibration of benzonitrile. *J. Phys. Chem. B* **2009**, *113*, 12736−12743.
(51) Kim, Y. S.; Hochstrasser, R. M. Chemical exchange 2D IR of hydrogen-bond making and breaking. *Proc. Natl. Acad. Sci. U. S. A.* **2005**, *102*, 11185−11190.
(52) van Wilderen, L. J. G. W.; Kern-Michler, D.; Müller-Werkmeister, H. M.; Bredenbeck, J. Vibrational dynamics and solvatochromism of the label SCN in various solvents and hemoglobin by time dependent IR and 2D-IR spectroscopy. *Phys. Chem. Chem. Phys.* **2014**, *16*, 19643−19653.
(53) Johnson, P. J. M.; Koziol, K. L.; Hamm, P. Intrinsic phasing of heterodyne-detected multidimensional infrared spectra. *Opt. Express* **2017**, *25*, 2928−2938.
(54) Yuan, R.; Yan, C.; Fayer, M. Ion−molecule complex dissociation and formation dynamics in LiCl aqueous solutions from 2D IR spectroscopy. *J. Phys. Chem. B* **2018**, *122*, 10582−10592.
(55) Yuan, R.; Fayer, M. D. Dynamics of water molecules and ions in concentrated lithium chloride solutions probed with ultrafast 2D IR spectroscopy. *J. Phys. Chem. B* **2019**, *123*, 7628−7639.
(56) Kramer, P. L.; Nishida, J.; Giammanco, C. H.; Tamimi, A.; Fayer, M. D. Observation and theory of reorientation-induced spectral diffusion in polarization-selective 2D IR spectroscopy. *J. Chem. Phys.* **2015**, *142*, 184505.
(57) Kwak, K.; Rosenfeld, D. E.; Fayer, M. D. Taking apart the two-dimensional infrared vibrational echo spectra: More information and elimination of distortions. *J. Chem. Phys.* **2008**, *128*, 204505.
(58) Kwak, K.; Park, S.; Finkelstein, I. J.; Fayer, M. D. Frequency-frequency correlation functions and apodization in two-dimensional infrared vibrational echo spectroscopy: A new approach. *J. Chem. Phys.* **2007**, *127*, 124503.
(59) Bagchi, S.; Boxer, S. G.; Fayer, M. D. Ribonuclease S dynamics measured using a nitrile label with 2D IR vibrational echo spectroscopy. *J. Phys. Chem. B* **2012**, *116*, 4034−4042.
(60) Ramos, S.; Le Sueur, A. L.; Horness, R. E.; Specker, J. T.; Collins, J. A.; Thibodeau, K. E.; Thielges, M. C. Heterogeneous and highly dynamic interface in plastocyanin−cytochrome f complex revealed by site-specific 2D-IR spectroscopy. *J. Phys. Chem. B* **2019**, *123*, 2114−2122.
(61) Urbanek, D. C.; Vorobyev, D. Y.; Serrano, A. L.; Gai, F.; Hochstrasser, R. M. The two-dimensional vibrational echo of a nitrile probe of the villin HP35 protein. *J. Phys. Chem. Lett.* **2010**, *1*, 3311−3315.
(62) Biava, H.; Schreiber, T.; Katz, S.; Völler, J.-S.; Stolarski, M.; Schulz, C.; Michael, N.; Budisa, N.; Kozuch, J.; Utesch, T.; Hildebrandt, P. Long-range modulations of electric fields in proteins. *J. Phys. Chem. B* **2018**, *122*, 8330−8342.
(63) Fafarman, A. T.; Webb, L. J.; Chuang, J. I.; Boxer, S. G. Site-specific conversion of cysteine thiols into thiocyanate creates an ir probe for electric fields in proteins. *J. Am. Chem. Soc.* **2006**, *128*, 13356−13357.
(64) Ramos, S.; Scott, K. J.; Horness, R. E.; Le Sueur, A. L.; Thielges, M. C. Extended timescale 2D IR probes of proteins: p-cyanoselenophenylalanine. *Phys. Chem. Chem. Phys.* **2017**, *19*, 10081−10086.
(65) Slocum, J. D.; Webb, L. J. Nitrile probes of electric field agree with independently measured fields in green fluorescent protein even in the presence of hydrogen bonding. *J. Am. Chem. Soc.* **2016**, *138*, 6561−6570.
(66) Dalton, S. R.; Vienneau, A. R.; Burstein, S. R.; Xu, R. J.; Linse, S.; Londergan, C. H. Cyanylated cysteine reports site-specific changes at protein−protein-binding interfaces without perturbation. *Biochemistry* **2018**, *57*, 3702−3712.
(67) Schmitz, A. J.; Hogle, D. G.; Gai, X. S.; Fenlon, E. E.; Brewer, S. H.; Tucker, M. J. Two-dimensional infrared study of vibrational

DOI: 10.1021/acs.jpcb.9b08954
J. Phys. Chem. B 2019, 123, 9355−9363

coupling between azide and nitrile reporters in a RNA nucleoside. *J. Phys. Chem. B* **2016**, *120*, 9387−9394.
(68) Bagchi, S.; Nebgen, B. T.; Loring, R. F.; Fayer, M. D. Dynamics of a myoglobin mutant enzyme: 2D IR vibrational echo experiments and simulations. *J. Am. Chem. Soc.* **2010**, *132*, 18367−18376.
(69) Fafarman, A. T.; Sigala, P. A.; Herschlag, D.; Boxer, S. G. Decomposition of vibrational shifts of nitriles into electrostatic and hydrogen-bonding effects. *J. Am. Chem. Soc.* **2010**, *132*, 12811−12813.
(70) Fried, S. D.; Bagchi, S.; Boxer, S. G. Extreme electric fields power catalysis in the active site of ketosteroid isomerase. *Science* **2014**, *346*, 1510−1514.
(71) Zhang, S.; Zhang, Y.; Ma, X.; Lu, L.; He, Y.; Deng, Y. Benzonitrile as a probe of local environment in ionic liquids. *J. Phys. Chem. B* **2013**, *117*, 2764−2772.
(72) Fried, S. D.; Boxer, S. G. Measuring electric fields and noncovalent interactions using the vibrational stark effect. *Acc. Chem. Res.* **2015**, *48*, 998−1006.
(73) Davari, N.; Daub, C. D.; Åstrand, P.-O.; Unge, M. Local field factors and dielectric properties of liquid benzene. *J. Phys. Chem. B* **2015**, *119*, 11839−11845.
(74) Schneider, S. H.; Boxer, S. G. Vibrational stark effects of carbonyl probes applied to reinterpret IR and raman data for enzyme inhibitors in terms of electric fields at the active site. *J. Phys. Chem. B* **2016**, *120*, 9672−9684.

DOI: 10.1021/acs.jpcb.9b08954
J. Phys. Chem. B 2019, 123, 9355−9363